bioRxiv preprint doi: https://doi.org/10.1101/781112; this version posted September 24, 2019. The copyright holder for this preprint (which was not certified by peer review) is the author/funder, who has granted bioRxiv a license to display the preprint in perpetuity. It is made available under aCC-BY 4.0 International license.

APOBEC3B reporter myeloma cell lines identify DNA damage response pathways leading to APOBEC3B expression

Hiroyuki Yamazaki[1], Kotaro Shirakawa[1], Tadahiko Matsumoto[1], Yasuhiro Kazuma[1], Hiroyuki Matsui[1], Yoshihito Horisawa[1], Emani Stanford[1], Anamaria Daniela Sarca[1], Ryutaro Shirakawa[2], Keisuke Shindo[1] and Akifumi Takaori-Kondo[1*]

From the [1]Department of Hematology and Oncology, Graduate School of Medicine, Kyoto University, Kyoto 606-8507, Japan, [2]Department of Molecular and Cellular Biology, Institute of Development, Aging and Cancer, Tohoku University, Sendai 980-8575, Japan.

***Correspondence:**

Akifumi Takaori-Kondo, MD, PhD

Department of Hematology and Oncology, Graduate School of Medicine, Kyoto University

54 Shogoin Kawahara-cho, Sakyo-ku, Kyoto 606-8507, Japan

Telephone: +81-75-751-4964

Fax: +81-75-751-4963

E-mail: atakaori@kuhp.kyoto-u.ac.jp

bioRxiv preprint doi: https://doi.org/10.1101/781112; this version posted September 24, 2019. The copyright holder for this preprint (which was not certified by peer review) is the author/funder, who has granted bioRxiv a license to display the preprint in perpetuity. It is made available under aCC-BY 4.0 International license.

19 **Text word count: 3635 words**

20 **Abstract word count: 190 words**

21 **Number of figures: 4**

22 **Number of tables: 0 (Supplemental Table: 2)**

23 **Number of references: 69**

bioRxiv preprint doi: https://doi.org/10.1101/781112; this version posted September 24, 2019. The copyright holder for this preprint (which was not certified by peer review) is the author/funder, who has granted bioRxiv a license to display the preprint in perpetuity. It is made available under aCC-BY 4.0 International license.

Abstract

Apolipoprotein B mRNA-editing enzyme catalytic polypeptide-like (APOBEC) DNA cytosine deaminase 3B (A3B) is a DNA editing enzyme which induces genomic DNA mutations in multiple myeloma and various other cancers. APOBEC family proteins are highly homologous so it is especially difficult to investigate the biology of A3B alone in cancer cells. To investigate A3B function in myeloma cells easily and comprehensively, we used CRISPR/Cas9 to generate A3B reporter cells that contain 3×FLAG tag and IRES-EGFP sequences integrated at the end of the A3B gene. These reporter cells stably express 3xFLAG tagged A3B and the reporter EGFP and this expression is enhanced under known stimuli, such as PMA. Conversely, shRNA knockdown of A3B decreased EGFP fluorescence and 3xFLAG tagged A3B protein levels. We screened a series of anticancer treatments using these cell lines and identified that most conventional therapies, such as antimetabolites or radiation, exacerbated endogenous A3B expression, but recent molecular targeting drugs, including bortezomib, lenalidomide and elotuzumab, did not. Furthermore, chemical inhibition of ATM, ATR and DNA-PK suppressed the EGFP expression upon treatment with antimetabolites. These results suggest that DNA damage response triggers A3B expression through ATM, ATR and DNA-PK signaling.

bioRxiv preprint doi: https://doi.org/10.1101/781112; this version posted September 24, 2019. The copyright holder for this preprint (which was not certified by peer review) is the author/funder, who has granted bioRxiv a license to display the preprint in perpetuity. It is made available under aCC-BY 4.0 International license.

Introduction

The apolipoprotein B mRNA-editing enzyme catalytic polypeptide-like DNA cytosine deaminase 3 family (APOBEC3, A3) consists of seven proteins (A3A, A3B, A3C, A3D, A3F, A3G and A3H) that preferentially induce C to U mutations in single strand DNA. A3 proteins were originally identified as factors of the innate immunity due to their mutagenic activity on viral genomes, and have recently joined the growing list of key intrinsic mutagens that play a part in oncogenesis [1]. Evidence for A3 mutagenicity consists in the presence of their mutational signature in cancer genomes [2], in the effects observed when overexpressed in tumor tissues [3, 4], as well as in the correlation of APOBEC signature mutations with poor prognosis [5, 6]. Nevertheless, the precise biology of individual APOBEC3 proteins in cancer cells remains unknown. Due to the high structural homology of APOBEC3 family members, it is particularly difficult to obtain high-affinity- and high-specificity- antibodies against each APOBEC3 protein, which limits our capability to distinguish the precise role of each endogenous APOBEC3 during tumorigenesis.

Among APOBEC3s, we previously reported that endogenous A3B is overexpressed and seems to be the main source of deamination activity in most of the myeloma cell lines we examined [7]. Notably, high levels of A3B expression in tumor cells were an independent risk factor for overall survival in myeloma patients [7] as well as in other cancer patients [8-11].

bioRxiv preprint doi: https://doi.org/10.1101/781112; this version posted September 24, 2019. The copyright holder for this preprint (which was not certified by peer review) is the author/funder, who has granted bioRxiv a license to display the preprint in perpetuity. It is made available under aCC-BY 4.0 International license.

However, the regulatory mechanisms that mediate A3B expression have not been well studied. To date, molecules including cell cycle pathway [12] and DNA damage response (DDR) [13, 14] factors and several transcription factors such as human papillomavirus E6/E7 [15, 16], NF-κB [17, 18], c-Maf [5] and B-Myb [19] were reported to enhance A3B expression. Nevertheless, how these factors mediate A3B expression and how A3B contributes to tumor progression and/or acquisition of chemoresistance in myeloma cells remains unclear. To investigate A3B-associated myeloma biology, we used the CRISPR/Cas9 system to introduce the 3×FLAG tag and IRES–EGFP gene at the beginning of the 3' UTR of the A3B gene in three human myeloma cell lines. We utilized this reporter cell lines to screen for how A3B expression is affected by anticancer treatments. Overall, we found these reporter cell lines to be very useful for the comprehensive analysis of A3B biology.

Materials and Methods

Human cell lines and culture

Three human myeloma cell lines, U266, RPMI8226 and AMO1 cells were maintained in RPMI1640 (Nacalai) containing 10% FBS and 1% PSG (Invitrogen). HEK293T and Lenti-X cells were maintained in DMEM (Nacalai) containing 10% FBS and 1% PSG (Invitrogen).

bioRxiv preprint doi: https://doi.org/10.1101/781112; this version posted September 24, 2019. The copyright holder for this preprint (which was not certified by peer review) is the author/funder, who has granted bioRxiv a license to display the preprint in perpetuity. It is made available under aCC-BY 4.0 International license.

78 **sgRNA design and construction of A3B reporter donor DNA**

79 To design the single-guide RNA (sgRNA) target sites, the mRNA sequence of APOBEC3B
80 (APOBEC3B Homo sapiens chromosome 22, GRCh38 Primary Assembly mRNA variant1, Fig.
81 1A) was imported into CRISPRdirect [20]. After a target site was determined, annealed oligos
82 (Supplemental Table 1) were inserted into pSpCas9(BB)–2A–Puro (PX459) V2.0 (Addgene,
83 #62988) using the *BbsI* (New England Biolabs) cloning site, or into lentiCRISPR ver.2
84 (Addgene, #52961) using the *BsmBI* (New England Biolabs) cloning site as previously described
85 [21, 22]. For the construction of the donor DNA plasmid (Fig. 1B), the right homology arm, the
86 modified cassette including 3×FLAG–IRES–EGFP gene and the left homology arm were PCR-
87 amplified using the KOD FX Neo (ToYoBo). Each PCR primer pair contained around 15 bp
88 overlaps. All the amplicons were cloned into a lentiviral plasmid pCSII–CMV–MCS (RIKEN,
89 RDB04377) by using the In-Fusion HD Cloning Kit (TaKaRa), to produce the pCSII–
90 CMV:A3B–3×FLAG–IRES–EGFP donor DNA plasmid.

91

92 **Validation of sgRNA targeting efficiency**

93 293T cells were transfected with pSpCas9(BB)–2A–Puro:sgRNA #4 (0.5 μg) using the FuGENE
94 HD Transfection Reagent (Promega). Two days after transfection, 293T cells were harvested and
95 their genomic DNA extracted using the QuickGene DNA whole blood kit S (KURABO). The

bioRxiv preprint doi: https://doi.org/10.1101/781112; this version posted September 24, 2019. The copyright holder for this preprint (which was not certified by peer review) is the author/funder, who has granted bioRxiv a license to display the preprint in perpetuity. It is made available under aCC-BY 4.0 International license.

96 targeted region was PCR-amplified from the genomic DNA using the targeting test primers
97 (Supplemental Table 1). The PCR products (200 ng) were denatured and then re-annealed to
98 form heteroduplex DNA. The hybridized DNA was digested with T7 endonuclease I (T7E1,
99 New England Biolabs), and run on 2% agarose gel. Mutation frequency was calculated based on
100 the band intensities, using Image J software, as previously described [23].
101
102 **Generation of A3B reporter cell lines**
103 For the U266 and AMO1 cell lines, 5×10^6 cells were co-transfected with 5 μg of pSpCas9(BB)–
104 2A–Puro:sgRNA #4 plasmid and 5 μg of pCSII–CMV:A3B–3×FLAG–IRES–EGFP donor DNA
105 plasmid using the Amaxa Nucleofector (Lonza) with nucleofection solution R, program X-001.
106 For the RPMI8226 cell line, 5×10^6 cells were transduced by the lentiCRISPR ver.2:sgRNA #4
107 viruses and the pCSII–CMV:A3B–3×FLAG–IRES–EGFP donor DNA viruses, simultaneously.
108 These lentiviruses were produced by co-transfection of the packaging plasmid pVSVg
109 (AddGene, #8454), psPAX2-D64V (AddGene, #63586) and lentiCRISPR ver.2:sgRNA #4
110 plasmid, or pCSII–CMV:A3B–3×FLAG–IRES–EGFP donor DNA plasmid, into Lenti-X cells.
111
112 **Flow cytometry analysis**

bioRxiv preprint doi: https://doi.org/10.1101/781112; this version posted September 24, 2019. The copyright holder for this preprint (which was not certified by peer review) is the author/funder, who has granted bioRxiv a license to display the preprint in perpetuity. It is made available under aCC-BY 4.0 International license.

Myeloma cells were stained with DRAQ7 (Biostatus) to mark dead cells, then were read on BD FACS Calibur or BD FACS Lyric (Becton-Dickinson Biosciences). To isolate A3B reporter cell lines, EGFP positive cells were sorted using a FACS Aria III cell sorter (Becton-Dickinson Biosciences) at seven days after transfection or transduction. Data were analyzed using the software FCSalyzer ver. 0.9.15-alpha. (https://sourceforge.net/projects/fcsalyzer/).

Genotyping of A3B reporter cell clones

Single clones were isolated from the sorted EGFP-positive cells of the three myeloma cell lines by limiting dilution. These clones were then PCR-genotyped using 2 pairs of the target confirmation primers, forward #a and reverse #b, and forward #c and reverse #b. To confirm the full sequence of A3B–3×FLAG–IRES–EGFP mRNA from the established cell line, complementary DNA (cDNA) was synthesized as described below, and was PCR-amplified by KOD FX Neo (ToYoBo) using a pair of primers, forward #d and reverse #e. The PCR products were sequenced using the 3130xl Genetic Analyzer (Applied Biosystems). All primers for PCR are listed in Supplemental Table 1.

Immunoblot analysis

bioRxiv preprint doi: https://doi.org/10.1101/781112; this version posted September 24, 2019. The copyright holder for this preprint (which was not certified by peer review) is the author/funder, who has granted bioRxiv a license to display the preprint in perpetuity. It is made available under aCC-BY 4.0 International license.

Whole cell lysates from 5.0×10^6 cells were prepared using SDS-based buffer (5 mM EDTA, 1% SDS) supplemented with Protease inhibitor cocktail (Roche) and PhosSTOP EASY (Roche), were mixed with an equal volume of twofold concentrated sample buffer (Bio-Rad Laboratories) containing β-mercaptoethanol (Nacalai Tesque), and were treated for 5 min at 100°C. Immunoblot analysis was performed as described previously using a mouse anti-FLAG antibody (Millipore, clone JBW301) or a mouse anti-α-tubulin monoclonal antibody (AA13, Funakoshi).

Immunofluorescence assays

Cells were air-dried and fixed in 4% paraformaldehyde in phosphate-buffered saline (PBS) for 20 minutes on glass slides using Shandon cytospin 2 (THERMO FISHER SCIENTIFIC). Fixed cells were permeabilized, reduced and denatured for 30 minutes in PBS buffer containing 0.5% SDS, 5% β-mercaptoethanol and 10% FBS. Then, cells were washed three times with PBS containing 4% FBS and 0.1% Triton X-100 (PFT buffer) [24], and incubated with a purified mouse anti-FLAG antibody for 1 hour. Subsequently, cells were incubated with a goat anti-mouse IgG (H+L)-Alexa Flour® 594 preadsorbed antibody (Abcam, ab150120) for 30 min in the dark. All antibodies were diluted with 3% BSA and 0.5% Tween in PBS. Then, the cells were stained with DAPI and were observed with a confocal laser scanning microscope (TCS-SP8, Leica).

bioRxiv preprint doi: https://doi.org/10.1101/781112; this version posted September 24, 2019. The copyright holder for this preprint (which was not certified by peer review) is the author/funder, who has granted bioRxiv a license to display the preprint in perpetuity. It is made available under aCC-BY 4.0 International license.

148

149 **Knockdown experiments**

150 We constructed pSicoR-mCherry lentiviral vectors [25] expressing short-hairpin RNA (shRNA)

151 against A3B by inserting synthetic double-stranded oligonucleotides, as previously described [7]

152 (TRCN0000140546 [26], sense oligo, 5'-

153 TGCAAAGCAATGTGCTCCTGATCTCGAGATCAGGAGCACATTGCTTTGCTTTTTTC-

154 3', and antisense oligo, 5'-

155 TCGAGAAAAAAGCAAAGCAATGTGCTCCTGATCTCGAGATCAGGAGCACATTGCTT

156 TGCA-3'; TRCN0000139463, sense oligo, 5'-

157 TCCTGATGGATCCAGACACATTCTCGAGAATGTGTCTGGATCCATCAGGTTTTTTC-

158 3', and antisense oligo, 5'-

159 TCGAGAAAAAACCTGATGGATCCAGACACATTCTCGAGAATGTGTCTGGATCCATCA

160 GGA-3') into the cloning site. For non-target shRNA, we used two constructs that were cloned

161 as scrambled sequences (control [27], sense oligo, 5'-

162 TGTCAAGTCTCACTTGCGTCTTCAAGAGAGACGCAAGTGAGACTTGACTTTTTTC-3',

163 antisense oligo, 5'-

164 TCGAGAAAAAAGTCAAGTCTCACTTGCGTCTCTCTTGAAGACGCAAGTGAGACTTGA

165 CA-3'; control-2 [28], sense oligo, 5'-

bioRxiv preprint doi: https://doi.org/10.1101/781112; this version posted September 24, 2019. The copyright holder for this preprint (which was not certified by peer review) is the author/funder, who has granted bioRxiv a license to display the preprint in perpetuity. It is made available under aCC-BY 4.0 International license.

166 TATCTCGCTTGGGCGAGAGTAAGCTCGAGCTTACTCTCGCCCAAGCGAGATTTTTTT

167 C-3', antisense oligo, 5'-

168 TCGAGAAAAAAATCTCGCTTGGGCGAGAGTAAGCTCGAGCTTACTCTCGCCCAAGC

169 GAGATA). The lentivirus was produced by co-transfection of Trans-Lentiviral packaging

170 plasmid mix (GE Dharmacon) and pSicoR-mCherry into Lenti-X cells.

171

172 **Quantitative RT-PCR**

173 Total RNA was extracted from cell lines using the High Pure RNA isolation kit (Roche). cDNA

174 was synthesized using the PrimeScriptR II 1st strand cDNA Synthesis Kit (Takara) by random

175 primer and oligo dT primer mixture. Real-time PCR was performed using the Thunderbird

176 SYBR qPCR Mix (ToYoBo). Target gene expression levels were normalized by endogenous

177 expression levels of HPRT1. All primers for real-time PCR are listed in Supplemental Table 1.

178

179 **Anticancer treatment screening**

180 To examine the effects of chemotherapeutic agents on A3B expression, the A3B reporter cells

181 were cultured for two days at a concentration of 2×10^5 cells/well/1.5 mL medium in 12-well

182 plates and treated with phorbol 12-myristate 13-acetate (PMA, Sigma), melphalan (MEL,

183 Wako), cisplatin (CDDP, Nihon-kayaku), mitomycin C (MMC, Funakoshi), N-desacetyl-N-

bioRxiv preprint doi: https://doi.org/10.1101/781112; this version posted September 24, 2019. The copyright holder for this preprint (which was not certified by peer review) is the author/funder, who has granted bioRxiv a license to display the preprint in perpetuity. It is made available under aCC-BY 4.0 International license.

184 methylocolchicine (COL, KaryoMAX Colcemid Solution in PBS, Thermo Fisher), camptothecin
185 (CPT-11, TopoGEN), etoposide (VP-16, TREVIGEN), cytosine-1-B-D(+)-arabinofuranoside
186 (Ara-C, Wako), gemcitabine hydrochloride (GEM, Sigma), hydroxyurea (HU, Tokyo chemical
187 industry), aphidicolin (APH, Wako), bortezomib (BOR, Funakoshi), lenalidomide (LEN, Sigma),
188 elotuzumab (ELO, Bristol-Myers Squibb), human IFN-α (Sumiferon, Dainippon Sumitomo
189 Pharma) and olaparib (Funakoshi) at several concentrations as described in the main text. These
190 chemotherapeutics were dissolved in 100 % dimethyl sulfoxide (Nacalai Tesque) with the
191 exception of COL, HU, ELO and INF-α which were dissolved in distilled water. To examine the
192 effects of radiation or UV on A3B expression, the cells were exposed to gamma irradiation using
193 a Cs-137 Gamma Cell or to UVC using a FUNA UV Crosslinker, FS-800 (Funakoshi). To
194 examine the effects of kinase inhibitors on A3B regulation, KU-55933 (Selleck), VE-821
195 (Selleck), NU-7026 (Selleck) and CGK733 (Calbiochem) were added 2 hours prior to
196 antimetabolite treatment.
197
198 **Statistical analysis**
199 Mann-Whitney U test and Welch's t test were calculated to evaluate the differences in
200 continuous variables between two groups in quantitative RT-PCR analysis and in flow cytometry

bioRxiv preprint doi: https://doi.org/10.1101/781112; this version posted September 24, 2019. The copyright holder for this preprint (which was not certified by peer review) is the author/funder, who has granted bioRxiv a license to display the preprint in perpetuity. It is made available under aCC-BY 4.0 International license.

201 analysis, respectively, by using the EZR software (version 3.0.2, Saitama Medical Center, Jichi
202 Medical University) [29].
203
204 **Results**
205 **CRISPR design**
206 We first designed candidates for sgRNA target sites in *A3B*, excluding introns, using the web
207 based tool, CRISPRdirect [20]. There are only four highly specific candidates for *A3B* (Fig. 1A
208 and Supplemental Table 2) mainly due to high homology among APOBEC3 family genes. In
209 order to insert the 3×FLAG sequence into *A3B* with a minimal off-target effect, we selected
210 sgRNA #4 (Fig.1A). We detected endogenous *A3B* overexpression in U266, RPMI8266 and
211 AMO1[7] and used the pSpCas9(BB)–2A–Puro plasmid and the lentiCRISPR ver.2 plasmid to
212 transduce CRISPR targeting *APOBEC3B* loci in these cell lines. We also used a donor DNA
213 template to introduce the 3×FLAG and IRES-EGFP reporter sequences at the end of the coding
214 region, while removing the stop codon (Figs. 1B and 1C). The 3×FLAG–IRES–EGFP cassette
215 was located adjacent to the beginning of 3' UTR, and intron 7 was removed to avoid partial gene
216 editing. Usually, the PAM sequence (NGG) in the donor DNA template must be mutated to
217 prevent cutting by cas9, however, in our case, any mutation of PAM would lead to alteration of
218 the A3B protein sequence. Instead, we designed six silent mutations within the target site to

bioRxiv preprint doi: https://doi.org/10.1101/781112; this version posted September 24, 2019. The copyright holder for this preprint (which was not certified by peer review) is the author/funder, who has granted bioRxiv a license to display the preprint in perpetuity. It is made available under aCC-BY 4.0 International license.

inhibit efficient sgRNA binding: the host genomic sequence of sgRNA #4, 'ctgGGACACCTTTGTGTACCGCCAGGgat', was altered to 'ctgGGACACGTTCGTCTATCGACAAGgat', in the donor DNA template sequence. Finally, the complete donor DNA template sequence was inserted into the pCSII–CMV–MCS plasmid in the opposite direction of the CMV promoter of the parental vector (Fig. 1C), so that cells in which the donor DNA vector is present merely transiently would not express *EGFP* and only cells which had their genome successfully engineered would emit EGFP fluorescent signals.

CRISPR guided 3×FLAG–IRES–EGFP insertion in *A3B* locus

To test the targeting efficiency of the sgRNA, we transfected pSpCas9(BB)–2A–Puro:sgRNA #4 plasmid into 293T cells. Transfection efficiency was 15.2% (T7E1 assay, Fig. 2A), therefore, we proceeded to co-transfect/co-transduce Cas9, the sgRNA #4 expressing vector and donor DNA vector into U266, RPMI8226 and AMO1 cell lines. As expected, the efficiency of genome editing in myeloma cells was quite low, but we successfully enriched EGFP positive cells by cell sorting (Fig. 2B). Single clones were isolated by limiting dilution from each cell line and genotyped. Finally, we established four knock-in cell lines from these single clones: U266$^{A3B–3\times FLAG–IRES–EGFP}$ #1 and #2 (U266 KI #1 and #2), RPMI8226$^{A3B–3\times FLAG–IRES–EGFP}$ (RPMI8226 KI), and AMO1$^{A3B–3\times FLAG–IRES–EGFP}$ (AMO1 KI). As indicated in Fig. 2C, the two genotype patterns

bioRxiv preprint doi: https://doi.org/10.1101/781112; this version posted September 24, 2019. The copyright holder for this preprint (which was not certified by peer review) is the author/funder, who has granted bioRxiv a license to display the preprint in perpetuity. It is made available under aCC-BY 4.0 International license.

237 suggest that the A3B–3×FLAG–IRES–EGFP cassette was correctly integrated at the target site in
238 these cell lines. Of note, U266 KI#2 lost both wild type alleles of *A3B* (Fig. 2C). To confirm the
239 mRNA sequence of A3B–3×FLAG–IRES–EGFP, we PCR-amplified the full length of the
240 cDNA derived from each cell line (Fig. 2D) and performed Sanger sequencing analysis. As
241 desired, all the engineered cell lines possessed correct A3B–3×FLAG sequences, with the
242 exception of the intended 6 silent mutations in the sgRNA target site and SNPs in the
243 unmanipulated region (Fig. 2E). According to flow cytometry analysis, the intensity of the
244 fluorescent signal increased in the order of U266 KI #1, RPMI8226 KI and AMO1 KI, which is
245 consistent with their A3B expression levels in a previous report [7]. U266 KI #2 exhibited
246 around two times stronger fluorescence than U266 KI #1, indicating that the 3×FLAG–IRES–
247 EGFP gene was integrated homozygously in U266 KI #2 and heterozygously in U266 KI #1.
248 According to the results of flow cytometry and PCR-genotyping (Fig. 2C), RPMI8226 KI and
249 AMO1 KI contain a single allele of the 3×FLAG–IRES–EGFP gene. Immunoblot analysis also
250 confirmed that all the cell lines produced A3B–3×FLAG proteins of the predicted size (Fig. 2G).
251 Immunofluorescent analysis of the subcellular localization of A3B–3×FLAG proteins showed a
252 dominant localization in the nucleoplasm (Fig, 2H), which is identical with that of intact A3B
253 proteins [7].
254

bioRxiv preprint doi: https://doi.org/10.1101/781112; this version posted September 24, 2019. The copyright holder for this preprint (which was not certified by peer review) is the author/funder, who has granted bioRxiv a license to display the preprint in perpetuity. It is made available under aCC-BY 4.0 International license.

The established A3B–3×FLAG–IRES–EGFP knock-in cell lines work as A3B reporters

To verify the feasibility of the established cell lines as A3B reporters, we first transduced RPMI8226 KI and AMO KI cells with lentiviral shRNA against A3B together with an EF1α-driven mCherry fluorescent marker. When A3B mRNA was efficiently depleted (Fig. 3A), A3B–3×FLAG protein levels decreased as expected (Fig. 3B). Similarly, EGFP fluorescent intensity decreased in mCherry positive, shRNA transduced cells, compared with mCherry negative, shRNA untransduced cells (Fig. 3C and 3D). Next, we treated U266 KI #1, RPMI8226 KI and AMO1 KI cells with PMA, a PKC activator, which is known to upregulate A3B expression via the NF-κB pathway [17, 18]. A quantitative RT-PCR analysis confirmed the enhancement of A3B mRNA levels for each cell line (Fig. 3E). Consistently, immunoblot analysis detects increases of A3B–3×FLAG proteins (Fig. 3F), and flow cytometry analysis detects peak shifts and increases of mean fluorescent intensity (MFI) for each cell line (Fig. 3G and 3H). Based on the above results, we conclude that these established cell lines properly work as A3B reporters.

DDR upregulates A3B expression via all the DDR-PIKK pathways in myeloma cells

Because the established A3B reporter cell lines provide an easy way to evaluate the alteration of A3B expression by simply performing flow cytometry analysis, we investigated which of the current clinically approved myeloma treatments affect A3B expression. Interestingly, most

bioRxiv preprint doi: https://doi.org/10.1101/781112; this version posted September 24, 2019. The copyright holder for this preprint (which was not certified by peer review) is the author/funder, who has granted bioRxiv a license to display the preprint in perpetuity. It is made available under aCC-BY 4.0 International license.

conventional anticancer treatments which induce DNA interstrand cross-links (e.g., CDDP, MEL and MMC), microtubule inhibition (e.g.,COL), topoisomerase inhibition (e.g.,CPT-11 and VP-16), DNA synthesis inhibition (e.g., Ara-C, GEM, HU and aphidicolin) or DNA double-strand breaks (e.g., radiation), exacerbated endogenous A3B overexpression (Fig. 4A and 4B). Treatment with olaparib alone, a Poly(ADP-ribose) polymerase (PARP) inhibitor, which is known to induce SSBs which are degraded to DSBs during replication [30], also enhanced A3B expression (Fig. 4C). On the other hand, the proteasome inhibitor (i.e., BOR), the immunomodulatory drug (i.e., LEN), the non-agonistic antibody drug (i.e., ELO) and INF-α did not enhance A3B expression levels (Fig.4A). These results intimate that DNA toxic stimulation upregulates A3B expression through DDR and following activation of DDR associated phosphatidylinositol 3' kinase-related kinases (DDR-PIKKs) [31] including ataxia telangiectasia and Rad3-related (ATR), and ataxia telangiectasia-mutated (ATM), DNA-dependent protein kinase (DNA-PK). Chemical inhibition of DDR-PIKKs by VE-821 for ATR, or NU-7026 for DNA-PK, suppressed EGFP increase upon antimetabolites treatment (Fig. 4D and 4E). Moreover, various combinations of PIKK inhibitors, including KU-55933, an ATM inhibitor, exhibited a synergistic effect of preventing A3B exacerbation upon antimetabolite stimulation (Fig.4D and 4E). Notably, pretreatment with CGK733 alone, which was first reported as an ATM/ATR inhibitor [32], almost completely blocked the antimetabolite effect on A3B

bioRxiv preprint doi: https://doi.org/10.1101/781112; this version posted September 24, 2019. The copyright holder for this preprint (which was not certified by peer review) is the author/funder, who has granted bioRxiv a license to display the preprint in perpetuity. It is made available under aCC-BY 4.0 International license.

291 expression in the three cell lines (Fig. 4F). These results suggest that all the DDR related
292 pathways are involved in A3B regulation in myeloma cells.
293
294 **Discussion**
295 In the present report, we successfully established four A3B reporter cell lines derived from three
296 human myeloma cell lines, U266, RPMI8226 and AMO1. These cell lines express EGFP
297 proteins with attribution to A3B expression, regulated by the same
298 transcriptional/posttranscriptional mechanisms due to identical promoter, the 3'-UTR and the 5'-
299 UTR to *A3B*. Due to these particularities, these cell lines are a very useful tool for investigating
300 A3B regulation in a high-throughput screening format by flow cytometry analysis, which will
301 allow for the development of specific A3B suppressors. There are several similar reports of other
302 gene-edited reporter cell lines used for comprehensively studying the transcriptional regulation
303 of the targeted gene [33-37]. In the case of A3B, most previous reports have studied A3B protein
304 function using exogenous overexpression by transient transfection in a limited number of cell
305 lines including non-human cells [16, 26, 38-44], mainly due to the difficulty of obtaining specific
306 anti-A3B antibodies. In contrast, the commercially available and certified anti-FLAG antibody
307 can be used to explore the A3B protein in the established A3B reporter cell lines described here.
308 That is to say, these cell lines have the potential to clarify natural protein-protein and/or DNA-

bioRxiv preprint doi: https://doi.org/10.1101/781112; this version posted September 24, 2019. The copyright holder for this preprint (which was not certified by peer review) is the author/funder, who has granted bioRxiv a license to display the preprint in perpetuity. It is made available under aCC-BY 4.0 International license.

309 protein interaction of A3B specifically, in tumor cells. In addition, the A3B reporter system can
310 be integrated into other A3B-overexpressing cell lines by using the Cas9/sgRNA #4 expressing
311 vector and pCSII–CMV:A3B–3×FLAG–IRES–EGFP donor DNA vector described here.
312 According to our pilot screening, most of the conventional anticancer treatments
313 exacerbated A3B overexpression in myeloma cells (Fig. 4A and 4B). These treatments seem to
314 act through a common pathway: induction of DDR [45]. Specifically, HU, which inhibits the
315 incorporation of nucleotides by interfering with the enzyme ribonucleotide reductase [46], and
316 APH, which interferes with DNA replication by inhibiting DNA polymerases α, ε and δ [47], are
317 both commonly used to induce replication fork stalling that leads to ATR/ATM activation. These
318 antimetabolites are also known to induce DSBs [48, 49]. CPT-11 covalently stabilizes the
319 topoisomerase I–DNA cleavage complex by inhibiting the religation of SSBs [50], thereby
320 increasing the number of SSBs and subsequent DSBs [51]. Meanwhile, VP-16 leads to increases
321 in the levels of topoisomerase II–DNA covalent complexes resulting in the rapid induction of
322 DSBs [52]. DNA interstrand cross-linkers form a number of adducts with DNA, and thereafter
323 activate a wide variety of DNA repair pathways [53] such as nucleotide excision repair (NER)
324 [54, 55], homology-directed repair (HDR) [56] and mismatch repair (MMR) [57]. DNA
325 interstrand cross-links are also known to be sensed by non-histone chromosomal high-mobility
326 group box proteins 1 and 2 (HMGB1 and HMGB2), which affect cell cycle events and

bioRxiv preprint doi: https://doi.org/10.1101/781112; this version posted September 24, 2019. The copyright holder for this preprint (which was not certified by peer review) is the author/funder, who has granted bioRxiv a license to display the preprint in perpetuity. It is made available under aCC-BY 4.0 International license.

subsequently induce apoptosis [58]. Colcemid also has the potential to induce DSBs [59, 60]. Although UV exposure dominantly produces cyclobutane pyrimidine dimers (CPDs) and 6-4 photoproducts (6-4PP) but not DSBs directly, it activates ATR by SSBs and ATM by DSBs in a NER-dependent manner [61]. On the other hand, bortezomib and lenalidomide did not enhance A3B overexpression (Fig. 4A). We cannot exclude the possibility that these drugs can directly cause DSBs, however, there are few reports of DNA damage induced by a single treatment with bortezomib or lenalidomide.

The upregulation of A3B expression induced by DNA damage was suppressed by DDR-PIKK inhibitors, consistent with a previous report in breast cancer [13]. Under single-inhibition of each DDR-PIKK pathway, the DNA-PK inhibitor (NU-7026) suppressed A3B elevation the strongest. Kanu et al. reported that inhibiting ATR, and to a lesser extent ATM, reduced the hydroxyurea-induced A3B activation, and concluded that DNA replication stress activates transcription of A3B via an ATR/Chk1-dependent pathway in breast cancer [13]. Thus, the dependency of A3B regulation on each DDR-PIKK pathway could vary among cancer cell types. On closer examination of the histograms in our study, EGFP signal curves from cells treated with NU-7026 had two peaks in contrast to those treated with VE-821 which had only one peak (Fig. 4D), suggesting that DNA-PK inhibition completely blocked A3B upregulation in a certain population of cells, whereas ATR inhibition suppressed it in all cells. Considering the synergistic

bioRxiv preprint doi: https://doi.org/10.1101/781112; this version posted September 24, 2019. The copyright holder for this preprint (which was not certified by peer review) is the author/funder, who has granted bioRxiv a license to display the preprint in perpetuity. It is made available under aCC-BY 4.0 International license.

345 effects of the combinations of DDR-PIKK inhibitors in our study (Fig. 4D and 4E), it seems that
346 all the DDR-PIKK pathways are at least partly involved in A3B regulation in myeloma cells.
347 This model is also supported by the redundancy between each DDR-PIKK pathway under DNA
348 replication stress [62]. Interestingly, A3B induction by DDR was almost completely blocked by
349 treatment with CGK733 alone. CGK733 was initially reported to inhibit both ATM and ATR
350 kinase activities, however, its specificity is now considered controversial [63, 64]. Nonetheless,
351 there seems to be no doubt that CGK733 targets at least partly a downstream factor of the
352 ATM/ATR pathway [65, 66]. HMGB1 and Cdc7 were identified as new target kinase candidates
353 of CGK733 [67]. Of note, proteasome inhibitors were reported to suppress DDR by inhibiting
354 phosphorylation of DDR-PIKKs [68, 69]. This suppression effect could explain why bortezomib
355 did not exacerbate A3B expression.

356 We previously reported that shRNA against A3B decreased the basal level of γH2AX
357 foci in myeloma cell lines, indicating that A3B induces constitutive DNA double-strand breaks,
358 promoting DDR activation [7]. Therefore DDR-inducible treatments trigger a positive feedback
359 loop for A3B expression, which may drive chemoresistant clone expansion during
360 chemotherapy. To prevent disease progression and potentiate current therapy, conventional
361 anticancer treatment coupled with a combination of DDR-PIKK inhibitors including a

bioRxiv preprint doi: https://doi.org/10.1101/781112; this version posted September 24, 2019. The copyright holder for this preprint (which was not certified by peer review) is the author/funder, who has granted bioRxiv a license to display the preprint in perpetuity. It is made available under aCC-BY 4.0 International license.

362 proteasome inhibitor might not only have a synergistic cytotoxicity for tumor cells but also
363 suppress the production of chemoresistant clones.
364
365 **Acknowledgments**
366 This work was partly supported by JSPS KAKENHI Grant numbers JP19H03502, 18H03992 for
367 A.T-K., JP19K07591 for K.S. and by AMED under Grant Number JP19ck0106250,
368 JP19cm0106501 for A.T-K.
369
370 **Competing Interests:** The authors declare no competing interests.
371
372 **Authorship Contributions**
373 H.Y., K.Shirakawa., and A.T.-K. conceived the study. H.Y. carried out experiments with help
374 from R.S., T.M., A.D.S., W.M., Y.K., H.M., H.F., Y.H., E.S., K.Shirakawa., K.Shindo. H.Y.,
375 K.Shirakawa., and A.T.-K. wrote the paper. All the authors reviewed and approved the
376 manuscript.
377
378 **References**
379 1. Henderson S, Fenton T. APOBEC3 genes: retroviral restriction factors to cancer drivers.

bioRxiv preprint doi: https://doi.org/10.1101/781112; this version posted September 24, 2019. The copyright holder for this preprint (which was not certified by peer review) is the author/funder, who has granted bioRxiv a license to display the preprint in perpetuity. It is made available under aCC-BY 4.0 International license.

380 Trends in molecular medicine. 2015;21(5):274-84.
381 2. Alexandrov LB, Nik-Zainal S, Wedge DC, Aparicio SA, Behjati S, Biankin AV, et al.
382 Signatures of mutational processes in human cancer. Nature. 2013;500(7463):415-21.
383 3. Swanton C, McGranahan N, Starrett GJ, Harris RS. APOBEC Enzymes: Mutagenic Fuel for
384 Cancer Evolution and Heterogeneity. Cancer Discov. 2015;5(7):704-12.
385 4. Gao J, Choudhry H, Cao W. Apolipoprotein B mRNA editing enzyme catalytic polypeptide-
386 like family genes activation and regulation during tumorigenesis. Cancer science. 2018;109(8):2375-
387 82.
388 5. Walker BA, Wardell CP, Murison A, Boyle EM, Begum DB, Dahir NM, et al. APOBEC family
389 mutational signatures are associated with poor prognosis translocations in multiple myeloma. Nat
390 Commun. 2015;6:6997.
391 6. Maura F, Petljak M, Lionetti M, Cifola I, Liang W, Pinatel E, et al. Biological and prognostic
392 impact of APOBEC-induced mutations in the spectrum of plasma cell dyscrasias and multiple
393 myeloma cell lines. Leukemia. 2018;32(4):1044-8.
394 7. Yamazaki H, Shirakawa K, Matsumoto T, Hirabayashi S, Murakawa Y, Kobayashi M, et al.
395 Endogenous APOBEC3B Overexpression Constitutively Generates DNA Substitutions and Deletions
396 in Myeloma Cells. Scientific reports. 2019;9(1).
397 8. Sieuwerts AM, Willis S, Burns MB, Look MP, Meijer-Van Gelder ME, Schlicker A, et al.
398 Elevated APOBEC3B correlates with poor outcomes for estrogen-receptor-positive breast cancers.
399 Hormones & cancer. 2014;5(6):405-13.
400 9. Law EK, Sieuwerts AM, LaPara K, Leonard B, Starrett GJ, Molan AM, et al. The DNA
401 cytosine deaminase APOBEC3B promotes tamoxifen resistance in ER-positive breast cancer. Science
402 advances. 2016;2(10):e1601737.
403 10. Yan S, He F, Gao B, Wu H, Li M, Huang L, et al. Increased APOBEC3B Predicts Worse
404 Outcomes in Lung Cancer: A Comprehensive Retrospective Study. J Cancer. 2016;7(6):618-25.
405 11. Du Y, Tao X, Wu J, Yu H, Yu Y, Zhao H. APOBEC3B up-regulation independently predicts
406 ovarian cancer prognosis: a cohort study. Cancer Cell Int. 2018;18:78.
407 12. Ng JCF, Quist J, Grigoriadis A, Malim MH, Fraternali F. Pan-cancer transcriptomic analysis
408 dissects immune and proliferative functions of APOBEC3 cytidine deaminases. Nucleic acids research.
409 2019.
410 13. Kanu N, Cerone MA, Goh G, Zalmas LP, Bartkova J, Dietzen M, et al. DNA replication stress
411 mediates APOBEC3 family mutagenesis in breast cancer. Genome biology. 2016;17(1):185.
412 14. Shimizu A, Fujimori H, Minakawa Y, Matsuno Y, Hyodo M, Murakami Y, et al. Onset of
413 deaminase APOBEC3B induction in response to DNA double-strand breaks. Biochem Biophys Rep.
414 2018;16:115-21.

bioRxiv preprint doi: https://doi.org/10.1101/781112; this version posted September 24, 2019. The copyright holder for this preprint (which was not certified by peer review) is the author/funder, who has granted bioRxiv a license to display the preprint in perpetuity. It is made available under aCC-BY 4.0 International license.

15. Vieira VC, Leonard B, White EA, Starrett GJ, Temiz NA, Lorenz LD, et al. Human papillomavirus E6 triggers upregulation of the antiviral and cancer genomic DNA deaminase APOBEC3B. mBio. 2014;5(6).

16. Mori S, Takeuchi T, Ishii Y, Kukimoto I. Identification of APOBEC3B promoter elements responsible for activation by human papillomavirus type 16 E6. Biochem Biophys Res Commun. 2015;460(3):555-60.

17. Leonard B, McCann JL, Starrett GJ, Kosyakovsky L, Luengas EM, Molan AM, et al. The PKC/NF-kappaB signaling pathway induces APOBEC3B expression in multiple human cancers. Cancer Res. 2015;75(21):4538-47.

18. Maruyama W, Shirakawa K, Matsui H, Matsumoto T, Yamazaki H, Sarca AD, et al. Classical NF-kappaB pathway is responsible for APOBEC3B expression in cancer cells. Biochem Biophys Res Commun. 2016;478(3):1466-71.

19. Chou WC, Chen WT, Hsiung CN, Hu LY, Yu JC, Hsu HM, et al. B-Myb Induces APOBEC3B Expression Leading to Somatic Mutation in Multiple Cancers. Scientific reports. 2017;7:44089.

20. Naito Y, Hino K, Bono H, Ui-Tei K. CRISPRdirect: software for designing CRISPR/Cas guide RNA with reduced off-target sites. Bioinformatics (Oxford, England). 2015;31(7):1120-3.

21. Ran FA, Hsu PD, Wright J, Agarwala V, Scott DA, Zhang F. Genome engineering using the CRISPR-Cas9 system. Nature protocols. 2013;8(11):2281-308.

22. Shalem O, Sanjana NE, Hartenian E, Shi X, Scott DA, Mikkelson T, et al. Genome-scale CRISPR-Cas9 knockout screening in human cells. Science (New York, NY). 2014;343(6166):84-7.

23. Guschin DY, Waite AJ, Katibah GE, Miller JC, Holmes MC, Rebar EJ. A rapid and general assay for monitoring endogenous gene modification. Methods in molecular biology (Clifton, NJ). 2010;649:247-56.

24. Blum R, Pfeiffer F, Feick P, Nastainczyk W, Kohler B, Schafer KH, et al. Intracellular localization and in vivo trafficking of p24A and p23. Journal of cell science. 1999;112 (Pt 4):537-48.

25. Salomonis N, Schlieve CR, Pereira L, Wahlquist C, Colas A, Zambon AC, et al. Alternative splicing regulates mouse embryonic stem cell pluripotency and differentiation. Proc Natl Acad Sci U S A. 2010;107(23):10514-9.

26. Burns MB, Lackey L, Carpenter MA, Rathore A, Land AM, Leonard B, et al. APOBEC3B is an enzymatic source of mutation in breast cancer. Nature. 2013;494(7437):366-70.

27. Hellman NE, Spector J, Robinson J, Zuo X, Saunier S, Antignac C, et al. Matrix metalloproteinase 13 (MMP13) and tissue inhibitor of matrix metalloproteinase 1 (TIMP1), regulated by the MAPK pathway, are both necessary for Madin-Darby canine kidney tubulogenesis. The Journal of biological chemistry. 2008;283(7):4272-82.

28. Eggenschwiler R, Loya K, Wu G, Sharma AD, Sgodda M, Zychlinski D, et al. Sustained

bioRxiv preprint doi: https://doi.org/10.1101/781112; this version posted September 24, 2019. The copyright holder for this preprint (which was not certified by peer review) is the author/funder, who has granted bioRxiv a license to display the preprint in perpetuity. It is made available under aCC-BY 4.0 International license.

450 knockdown of a disease-causing gene in patient-specific induced pluripotent stem cells using lentiviral
451 vector-based gene therapy. Stem cells translational medicine. 2013;2(9):641-54.
452 29. Kanda Y. Investigation of the freely available easy-to-use software 'EZR' for medical statistics.
453 Bone marrow transplantation. 2013;48(3):452-8.
454 30. Li M, Yu X. The role of poly(ADP-ribosyl)ation in DNA damage response and cancer
455 chemotherapy. Oncogene. 2015;34(26):3349-56.
456 31. Blackford AN, Jackson SP. ATM, ATR, and DNA-PK: The Trinity at the Heart of the DNA
457 Damage Response. Molecular cell. 2017;66(6):801-17.
458 32. Won J, Kim M, Kim N, Ahn JH, Lee WG, Kim SS, et al. Small molecule-based reversible
459 reprogramming of cellular lifespan. Nature chemical biology. 2006;2(7):369-74.
460 33. Cho YS, Kim BS, Sim CK, Kim I, Lee MS. Establishment of IL-7 Expression Reporter Human
461 Cell Lines, and Their Feasibility for High-Throughput Screening of IL-7-Upregulating Chemicals.
462 PLoS One. 2016;11(9):e0161899.
463 34. Shan L, Wang D, Mao Q, Xia H. Establishment of a DGKtheta Endogenous Promoter
464 Luciferase Reporter HepG2 Cell Line for Studying the Transcriptional Regulation of DGKtheta Gene.
465 Applied biochemistry and biotechnology. 2019;187(4):1344-55.
466 35. Li Z, Zhao J, Muhammad N, Wang D, Mao Q, Xia H. Establishment of a HEK293 cell line by
467 CRISPR/Cas9-mediated luciferase knock-in to study transcriptional regulation of the human SREBP1
468 gene. Biotechnology letters. 2018;40(11-12):1495-506.
469 36. Veach RA, Wilson MH. CRISPR/Cas9 engineering of a KIM-1 reporter human proximal
470 tubule cell line. PLoS One. 2018;13(9):e0204487.
471 37. Li Y, Li S, Li Y, Xia H, Mao Q. Generation of a novel HEK293 luciferase reporter cell line by
472 CRISPR/Cas9-mediated site-specific integration in the genome to explore the transcriptional
473 regulation of the PGRN gene. Bioengineered. 2019;10(1):98-107.
474 38. Shinohara M, Io K, Shindo K, Matsui M, Sakamoto T, Tada K, et al. APOBEC3B can impair
475 genomic stability by inducing base substitutions in genomic DNA in human cells. Scientific reports.
476 2012;2:806.
477 39. Taylor BJ, Nik-Zainal S, Wu YL, Stebbings LA, Raine K, Campbell PJ, et al. DNA deaminases
478 induce break-associated mutation showers with implication of APOBEC3B and 3A in breast cancer
479 kataegis. Elife. 2013;2:e00534.
480 40. Akre MK, Starrett GJ, Quist JS, Temiz NA, Carpenter MA, Tutt AN, et al. Mutation
481 Processes in 293-Based Clones Overexpressing the DNA Cytosine Deaminase APOBEC3B. PLoS One.
482 2016;11(5):e0155391.
483 41. Hoopes JI, Cortez LM, Mertz TM, Malc EP, Mieczkowski PA, Roberts SA. APOBEC3A and
484 APOBEC3B Preferentially Deaminate the Lagging Strand Template during DNA Replication. Cell

bioRxiv preprint doi: https://doi.org/10.1101/781112; this version posted September 24, 2019. The copyright holder for this preprint (which was not certified by peer review) is the author/funder, who has granted bioRxiv a license to display the preprint in perpetuity. It is made available under aCC-BY 4.0 International license.

Rep. 2016;14(6):1273-82.

42. Zhang W, Zhang X, Tian C, Wang T, Sarkis PT, Fang Y, et al. Cytidine deaminase APOBEC3B interacts with heterogeneous nuclear ribonucleoprotein K and suppresses hepatitis B virus expression. Cellular microbiology. 2008;10(1):112-21.

43. Xiao X, Yang H, Arutiunian V, Fang Y, Besse G, Morimoto C, et al. Structural determinants of APOBEC3B non-catalytic domain for molecular assembly and catalytic regulation. Nucleic acids research. 2017;45(12):7494-506.

44. Mishra N, Reddy KS, Timilsina U, Gaur D, Gaur R. Human APOBEC3B interacts with the heterogenous nuclear ribonucleoprotein A3 in cancer cells. Journal of cellular biochemistry. 2018;119(8):6695-703.

45. Vesela E, Chroma K, Turi Z, Mistrik M. Common Chemical Inductors of Replication Stress: Focus on Cell-Based Studies. Biomolecules. 2017;7(1).

46. Krakoff IH, Brown NC, Reichard P. Inhibition of ribonucleoside diphosphate reductase by hydroxyurea. Cancer Res. 1968;28(8):1559-65.

47. Cheng CH, Kuchta RD. DNA polymerase epsilon: aphidicolin inhibition and the relationship between polymerase and exonuclease activity. Biochemistry. 1993;32(33):8568-74.

48. Saintigny Y, Delacote F, Vares G, Petitot F, Lambert S, Averbeck D, et al. Characterization of homologous recombination induced by replication inhibition in mammalian cells. The EMBO journal. 2001;20(14):3861-70.

49. Ewald B, Sampath D, Plunkett W. H2AX phosphorylation marks gemcitabine-induced stalled replication forks and their collapse upon S-phase checkpoint abrogation. Molecular cancer therapeutics. 2007;6(4):1239-48.

50. Staker BL, Hjerrild K, Feese MD, Behnke CA, Burgin AB, Jr., Stewart L. The mechanism of topoisomerase I poisoning by a camptothecin analog. Proc Natl Acad Sci U S A. 2002;99(24):15387-92.

51. Tuduri S, Crabbe L, Conti C, Tourriere H, Holtgreve-Grez H, Jauch A, et al. Topoisomerase I suppresses genomic instability by preventing interference between replication and transcription. Nature cell biology. 2009;11(11):1315-24.

52. Nitiss JL. Targeting DNA topoisomerase II in cancer chemotherapy. Nature reviews Cancer. 2009;9(5):338-50.

53. Dronkert ML, Kanaar R. Repair of DNA interstrand cross-links. Mutation research. 2001;486(4):217-47.

54. Koberle B, Masters JR, Hartley JA, Wood RD. Defective repair of cisplatin-induced DNA damage caused by reduced XPA protein in testicular germ cell tumours. Current biology : CB. 1999;9(5):273-6.

55. Damsma GE, Alt A, Brueckner F, Carell T, Cramer P. Mechanism of transcriptional stalling

bioRxiv preprint doi: https://doi.org/10.1101/781112; this version posted September 24, 2019. The copyright holder for this preprint (which was not certified by peer review) is the author/funder, who has granted bioRxiv a license to display the preprint in perpetuity. It is made available under aCC-BY 4.0 International license.

520 at cisplatin-damaged DNA. Nat Struct Mol Biol. 2007;14(12):1127-33.
521 56. Borst P, Rottenberg S, Jonkers J. How do real tumors become resistant to cisplatin? Cell cycle
522 (Georgetown, Tex). 2008;7(10):1353-9.
523 57. Sedletska Y, Fourrier L, Malinge JM. Modulation of MutS ATP-dependent functional
524 activities by DNA containing a cisplatin compound lesion (base damage and mismatch). Journal of
525 molecular biology. 2007;369(1):27-40.
526 58. Brown R, Clugston C, Burns P, Edlin A, Vasey P, Vojtesek B, et al. Increased accumulation
527 of p53 protein in cisplatin-resistant ovarian cell lines. International journal of cancer. 1993;55(4):678-
528 84.
529 59. Hayashi MT, Cesare AJ, Fitzpatrick JA, Lazzerini-Denchi E, Karlseder J. A telomere-
530 dependent DNA damage checkpoint induced by prolonged mitotic arrest. Nat Struct Mol Biol.
531 2012;19(4):387-94.
532 60. Li H, Chang TW, Tsai YC, Chu SF, Wu YY, Tzang BS, et al. Colcemid inhibits the rejoining
533 of the nucleotide excision repair of UVC-induced DNA damages in Chinese hamster ovary cells.
534 Mutation research. 2005;588(2):118-28.
535 61. Wakasugi M, Sasaki T, Matsumoto M, Nagaoka M, Inoue K, Inobe M, et al. Nucleotide
536 excision repair-dependent DNA double-strand break formation and ATM signaling activation in
537 mammalian quiescent cells. The Journal of biological chemistry. 2014;289(41):28730-7.
538 62. Stiff T, Walker SA, Cerosaletti K, Goodarzi AA, Petermann E, Concannon P, et al. ATR-
539 dependent phosphorylation and activation of ATM in response to UV treatment or replication fork
540 stalling. The EMBO journal. 2006;25(24):5775-82.
541 63. Choi S, Toledo LI, Fernandez-Capetillo O, Bakkenist CJ. CGK733 does not inhibit ATM or
542 ATR kinase activity in H460 human lung cancer cells. DNA repair. 2011;10(10):1000-1; author reply
543 2.
544 64. Williams TM, Nyati S, Ross BD, Rehemtulla A. Molecular imaging of the ATM kinase activity.
545 Int J Radiat Oncol Biol Phys. 2013;86(5):969-77.
546 65. Fallone F, Britton S, Nieto L, Salles B, Muller C. ATR controls cellular adaptation to hypoxia
547 through positive regulation of hypoxia-inducible factor 1 (HIF-1) expression. Oncogene.
548 2013;32(37):4387-96.
549 66. Bhattacharya S, Ray RM, Johnson LR. Role of polyamines in p53-dependent apoptosis of
550 intestinal epithelial cells. Cellular signalling. 2009;21(4):509-22.
551 67. Suzuki T, Tsuzuku J, Hayashi A, Shiomi Y, Iwanari H, Mochizuki Y, et al. Inhibition of DNA
552 damage-induced apoptosis through Cdc7-mediated stabilization of Tob. The Journal of biological
553 chemistry. 2012;287(48):40256-65.
554 68. Sakasai R, Teraoka H, Tibbetts RS. Proteasome inhibition suppresses DNA-dependent

bioRxiv preprint doi: https://doi.org/10.1101/781112; this version posted September 24, 2019. The copyright holder for this preprint (which was not certified by peer review) is the author/funder, who has granted bioRxiv a license to display the preprint in perpetuity. It is made available under aCC-BY 4.0 International license.

protein kinase activation caused by camptothecin. DNA repair. 2010;9(1):76-82.

69. Jacquemont C, Taniguchi T. Proteasome function is required for DNA damage response and fanconi anemia pathway activation. Cancer Res. 2007;67(15):7395-405.

bioRxiv preprint doi: https://doi.org/10.1101/781112; this version posted September 24, 2019. The copyright holder for this preprint (which was not certified by peer review) is the author/funder, who has granted bioRxiv a license to display the preprint in perpetuity. It is made available under aCC-BY 4.0 International license.

560 **Figure Legends**

561 **Figure 1.** Schema of APOBEC3B editing strategy. (**A**) Schema of A3B mRNA structure.
562 Triangles indicate highly-specific sgRNA target sites for *A3B*. Each intermittent arrow represents
563 an exon (Ex). Areas in light gray show UTRs, those in dark gray show coding sequence regions
564 (CDRs), and those in blue show catalytic domains. The mRNA of A3B isoforms (arrows in
565 orange) as well as shA3B target sites (rectangles in yellow) are also indicated. (**B**) Schema of
566 *A3B* in the host genome and in the donor DNA template. The donor DNA template contains six
567 silent mutations in the sgRNA #4 target site, and intron 6 was removed. The 3×FLAG–IRES–
568 EGFP sequence was inserted adjacent to the beginning of 3' UTR. (**C**) Schema of donor DNA
569 plasmid, pCSII–CMV:A3B–3×FLAG–IRES–EGFP.

570

571 **Figure 2.** Establishment of A3B–3×FLAG–IRES–EGFP knock-in myeloma cell lines. (**A**) T7E1
572 assay of the sgRNA #4 site in 293T cells. Expected positions of uncleaved (606 bp) and cleaved
573 (532 bp and 74 bp) DNA bands by T7E1 are indicated with arrows. The mutation frequency is
574 also shown. (**B**) Flow cytometry of U266, RPMI8226 and AMO1 cells after introduction of the
575 donor DNA vector along with the CRISPR-Cas9 vector. EGFP positive cells are highlighted in
576 green and their proportions are indicated. (**C**) Genotyping PCR for genomic DNA from each
577 clone derived from a single cell among the enriched cells in (B). Each clone was genotyped by

bioRxiv preprint doi: https://doi.org/10.1101/781112; this version posted September 24, 2019. The copyright holder for this preprint (which was not certified by peer review) is the author/funder, who has granted bioRxiv a license to display the preprint in perpetuity. It is made available under aCC-BY 4.0 International license.

two pairs of primers, Fw #a × Rv #b and Fw #c × Rv #b. Using the former primer pair, the expected size of the PCR amplicon is 2109 bp for the intact allele, and 3225 bp for the knock-in allele. Using the latter primer pair, the PCR amplicon (2349 bp) can be detected only if the knock-in allele is present. (**D**) Genotyping PCR for cDNA from each clone in (C). The PCR amplicon (2401 bp) can be detected only if the knock-in allele is present. (**E**) Sanger sequencing results for the full length of the edited A3B cDNA originated from the clones of 3×FLAG–IRES–EGFP knock-in cell lines. Schema of the A3B–3×FLAG–IRES–EGFP mRNA structure is also depicted, the same as in Fig.1B. (**F**) Histograms of EGFP intensity values from the 3×FLAG–IRES–EGFP knock-in cell lines as determined by flow cytometry. (**G**) Immunoblot analysis of the 3×FLAG–IRES–EGFP knock-in cell lines. α-tubulin was evaluated as internal control. (**H**) Immunofluorescence analysis of the 3×FLAG–IRES–EGFP knock-in clones using an anti-FLAG antibody. For U226 KI, clone U266 KI #1 was examined. Images were obtained by confocal fluorescence microscopy (magnification, x630).

Figure 3. A3B–3×FLAG–IRES–EGFP knock-in cells work as A3B reporters. (**A**, **B**) Real-time PCR (A) and immunoblotting (B) of A3B in RPMI8226 KI cells and AMO1 KI cells, which were transduced with lentiviral shRNA against A3B (two constructs: shA3B or shA3B-2) or control (two constructs: control or control-2). HPRT1 or α-tubulin were evaluated as internal

bioRxiv preprint doi: https://doi.org/10.1101/781112; this version posted September 24, 2019. The copyright holder for this preprint (which was not certified by peer review) is the author/funder, who has granted bioRxiv a license to display the preprint in perpetuity. It is made available under aCC-BY 4.0 International license.

596 controls. (**C**, **D**) Flow cytometry of RPMI8226 KI cells (C) and AMO1 KI cells (D) at 17 days
597 after transduction with lentiviral shRNA against A3B or control. In the histogram representation,
598 EGFP intensity was compared between mCherry positive cells (colored in red) and mCherry
599 negative cells (colored in green). (**E**, **F**) Real-time PCR (E) and immunoblotting (F) of A3B in
600 three A3B–3×FLAG–IRES–EGFP knock-in cell lines, which were treated with PMA (20 ng/mL)
601 for 6 hours and 24 hours, respectively. (**G**) Representative result of EGFP intensity histogram of
602 AMO1 KI cells, which were treated with PMA (20 ng/mL) for 2 days. (**H**) Bar graph of EGFP
603 mean fluorescent intensity (MFI) of three A3B–3×FLAG–IRES–EGFP knock-in cell lines,
604 which were treated with PMA (20 ng/mL) for 2 days.
605
606 **Figure 4.** DNA damage response exacerbates A3B overexpression via the DDR-PIKK pathways
607 in myeloma cells. (**A**) A panel of EGFP mean fluorescent intensity (MFI) of three A3B–
608 3×FLAG–IRES–EGFP knock-in cell lines with various anti-cancer treatment. The A3B reporter
609 cells were incubated for 2 days with each anti-cancer reagent at the concentrations indicated on
610 the horizontal axis. For the UVC exposure experiment, the A3B reporter cells were irradiated
611 with a single dose at 2 days before flow cytometry analysis. Hash mark (#) represents
612 unmeasurable state due to cytotoxicity. (**B**) Bar graph of EGFP MFI of AMO1 KI cells, which
613 were exposed to a single dose of γ-ray at 2 days before flow cytometry analysis. (**C**) Bar graph of

bioRxiv preprint doi: https://doi.org/10.1101/781112; this version posted September 24, 2019. The copyright holder for this preprint (which was not certified by peer review) is the author/funder, who has granted bioRxiv a license to display the preprint in perpetuity. It is made available under aCC-BY 4.0 International license.

614 EGFP MFI of three A3B–3×FLAG–IRES–EGFP knock-in cell lines with olaparib treatment (10
615 μM) for 2 days. (**D**, **E**) Histograms (D) and bar graphs (E) of EGFP intensity values from AMO1
616 KI cells, which were co-treated with HU (1μM) and DDR-PIKK inhibitors: KU-55933, 5 μM;
617 VE-821, 5 μM; NU-7026, 2 μM; CGK733, 5 μM. Cells were incubated with the reagents for 2
618 days and subsequently analyzed by flow cytometry. (**F**) Bar graph of EGFP MFI of three A3B–
619 3×FLAG–IRES–EGFP knock-in cell lines treated with an antimetabolite (Ara-C, 50 μM; GEM,
620 1 μM; HU, 1 μM) with or without CGK733 (5 μM) for 2 days.
621
622 **Supplemental Table 1.** List of oligos and thermal cycle conditions for genotyping PCR.
623
624 **Supplemental Table 2.** sgRNA target candidates for A3B.
625

Figure 1

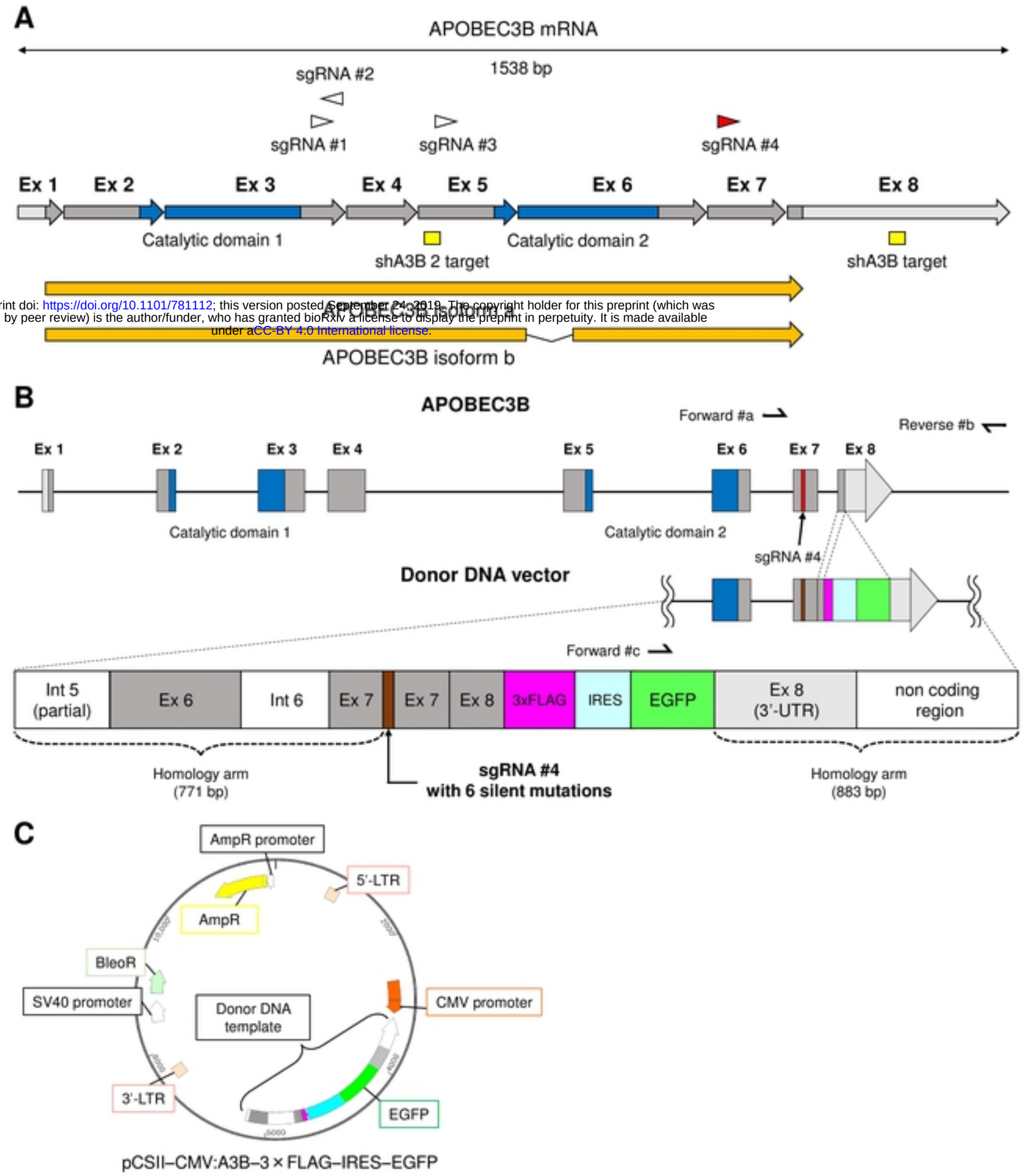

bioRxiv preprint doi: https://doi.org/10.1101/781112; this version posted September 24, 2019. The copyright holder for this preprint (which was not certified by peer review) is the author/funder, who has granted bioRxiv a license to display the preprint in perpetuity. It is made available under aCC-BY 4.0 International license.

Figure 2

bioRxiv preprint doi: https://doi.org/10.1101/781112; this version posted September 24, 2019. The copyright holder for this preprint (which was not certified by peer review) is the author/funder, who has granted bioRxiv a license to display the preprint in perpetuity. It is made available under aCC-BY 4.0 International license.

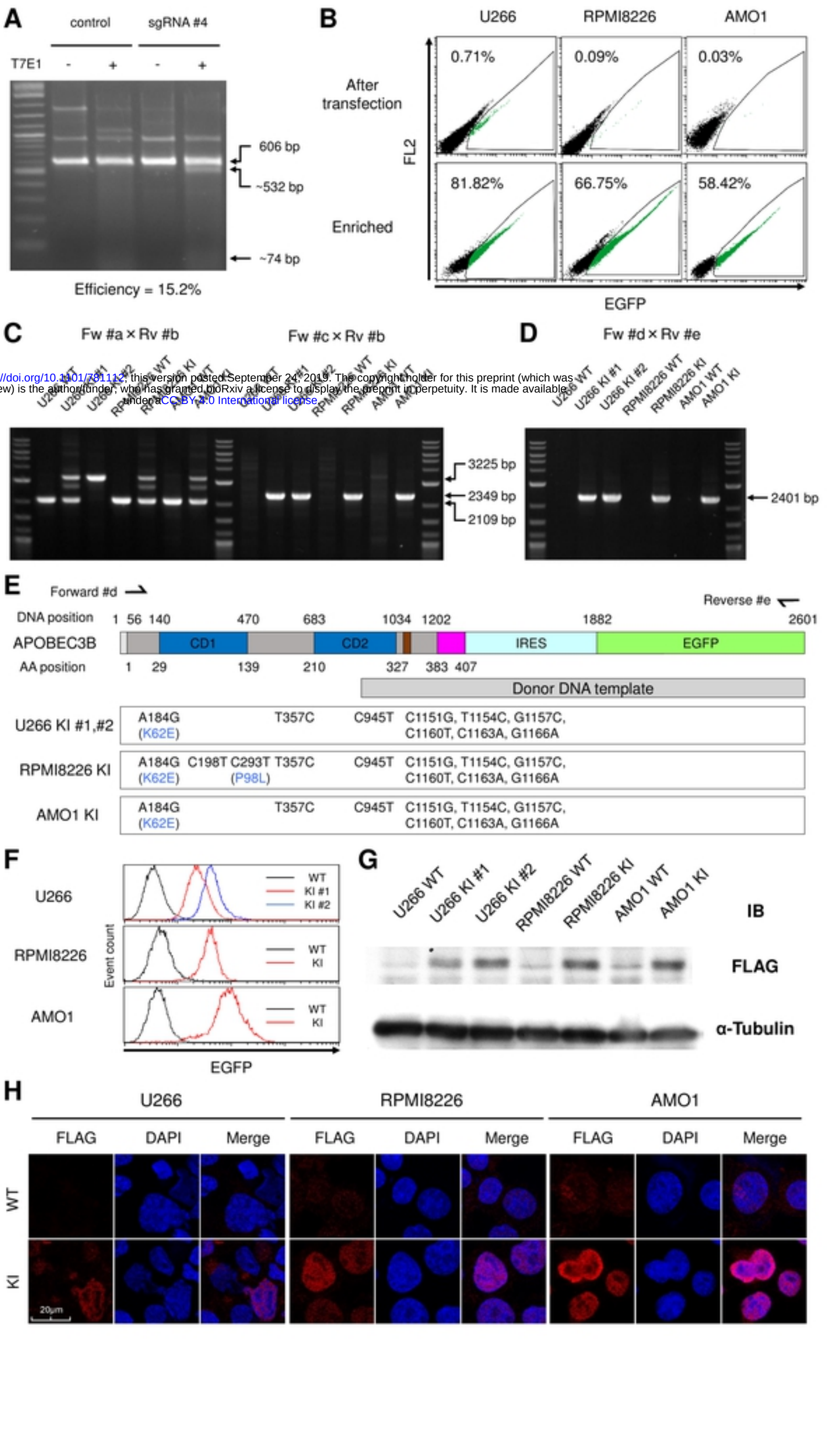

Figure 3

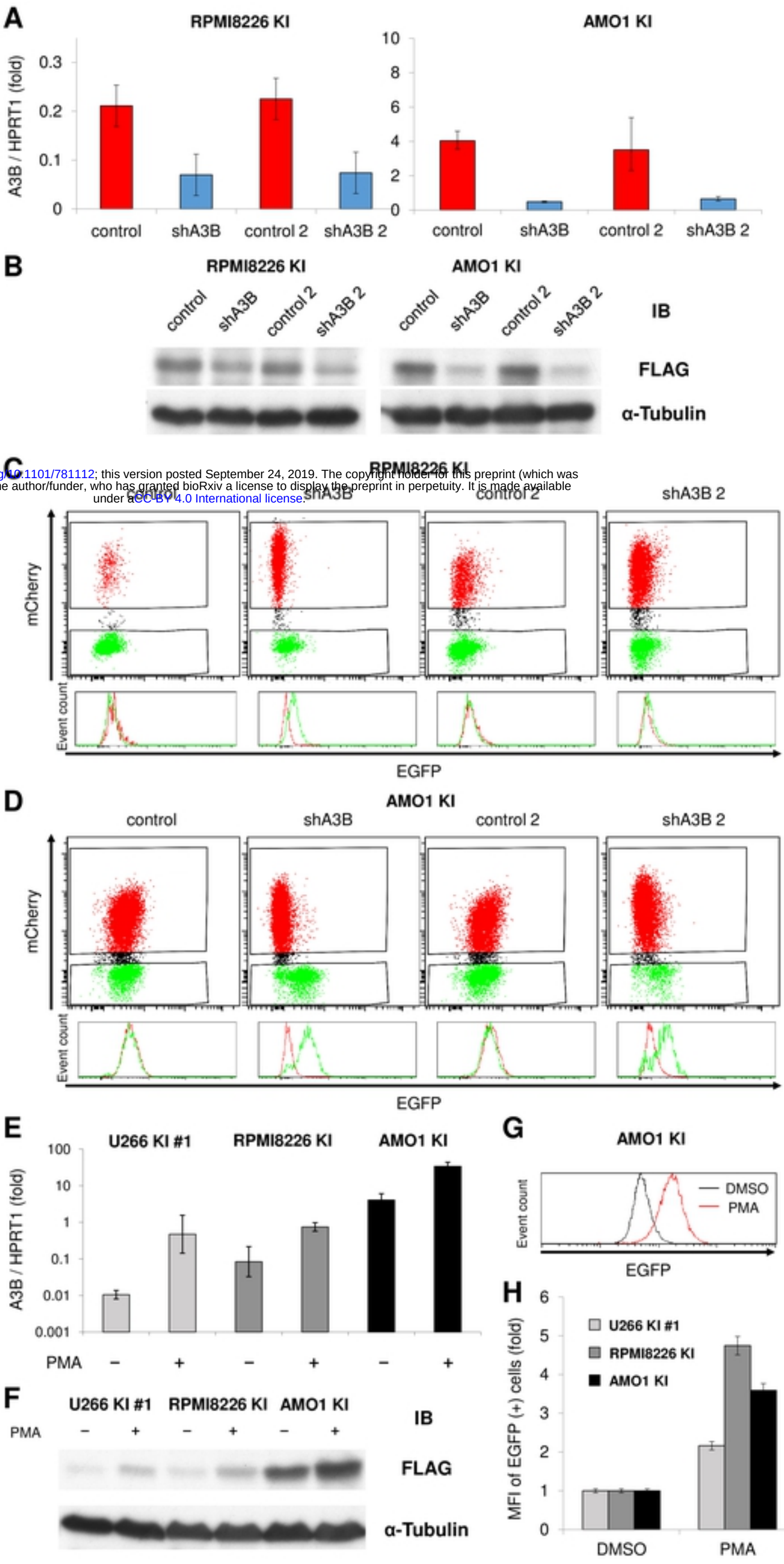

bioRxiv preprint doi: https://doi.org/10.1101/781112; this version posted September 24, 2019. The copyright holder for this preprint (which was not certified by peer review) is the author/funder, who has granted bioRxiv a license to display the preprint in perpetuity. It is made available under a CC-BY 4.0 International license.

bioRxiv preprint doi: https://doi.org/10.1101/781112; this version posted September 24, 2019. The copyright holder for this preprint (which was not certified by peer review) is the author/funder, who has granted bioRxiv a license to display the preprint in perpetuity. It is made available under aCC-BY 4.0 International license.

Figure 4